display

CLM-P245

United Kingdom Atomic Energy Authority
RESEARCH GROUP

Preprint

THE MAGNETIC WELL EXPERIMENT M.T.S.E. 11

D. E. T. F. ASHBY
E. L. BYDDER
G. FRANCIS
J. W. HILL
M. H. HUGHES
D. W. MASON

Culham Laboratory
Abingdon Berkshire

1970

CLM - P 245

THE MAGNETIC WELL EXPERIMENT M.T.S.E. II

by

D.E.T.F. ASHBY, E.L. BYDDER, G. FRANCIS*,

J.W. HILL, M.H. HUGHES and D.W. MASON

(To be submitted for publication in Nuclear Fusion)

ABSTRACT

Experiments with a magnetic well using a gun-injected plasma are described. Typical parameters are $B_z \simeq 1{\cdot}8$ kG, $n = 5 \times 10^{12}$ cm^{-3}, $T_i = 1{\cdot}5$ keV, $T_e = 15$ eV and length of trap = 1·5 m. A wide range of diagnostics have been used including atomic beams of K, Kr and Xe for measuring $\int n d\ell$ and T_e. An initial rapid loss of plasma is associated with the method of filling the trap which results in an ion velocity space distribution peaking near the loss cone angle; however, detailed analysis shows that the ion scattering process is not caused by Coulomb collisions although the energy transfer rate between ions and electrons is not inconsistent with classical collisions. Electric field fluctuations of ~ 1 V cm^{-1} near ω_{ci} are observed which appear to be associated with the anomalous ion scattering.

*Dr Gordon Francis, who initiated and led the M.T.S.E. series of experiments, died in January 1969 and failed to see the culmination of his work.

U.K.A.E.A. Research Group,
Culham Laboratory
Abingdon
Berks

July, 1970

1. INTRODUCTION

Since Ioffe's[1] original work several other experiments (e.g. refs.2-4) have confirmed that plasma contained adiabatically in a magnetic well is stable against interchange instabilities. The theory underlying this stability has been developed e.g. Taylor[5,6]. Interest has subsequently been focussed on various microinstabilities which can occur in mirror machines[7-9]. Experimentally such microinstabilities have been investigated most extensively in low density mirror machines employing particle injection, (e.g refs. 10,11) but instabilities have also been observed and studied in the magnetic well 2X which uses a dense plasma produced by plasma injection[12]. The requirements of an economic fusion reactor have stimulated interest in the behaviour of dense plasmas[13], where ideally the particle energy density approaches the magnetic energy density (i.e. high β where $\beta = 2\mu_0 nkT/B^2$). An economic fusion reactor, based on a magnetic well, becomes impossible if the ion scattering rate is essentially greater than that caused by Coulomb collisions; consequently, any increase in ion loss rate due to anomalous scattering at high β is of great consequence for magnetic wells.

The initial well experiments on M.T.S.E. I (the forerunner of the experimental apparatus described in this paper) used a low density gun-injected plasma with approximately 4×10^{10} ions cm^{-3}[4]. Subsequent experiments with a density of 10^{13} ions cm^{-3}[14] indicated that the apparatus was unsuitable for experiments at this density due to the influx of neutrals resulting from wall bombardment by escaping particles.

The present apparatus (the Magnetic Trap Stability Experiment II called M.T.S.E. II) was designed for high density experiments.

The vacuum walls are gettered with evaporated titanium and placed approximately 70 cm from the confined plasma to reduce the effect of desorbed gas. The main machine parameters minimise cost while being consistent with adiabaticity and a substantial difference between the rate of plasma loss by ion-ion collisions and charge exchange. They are as follows:

magnetic flux density $B_z = 1{\cdot}8$ kG;

plasma density $n \simeq 5 \times 10^{12}$ cm^{-3};

mean ion energy $W_i = 1\text{-}2$ keV.

The results of intial experiments on M.T.S.E. II were described at Novosibirsk[15]. The main feature of these results was that the trapped plasma was grossly stable and showed no detectable electric potential fluctuations, the confinement time measured by fast atom emission was about an order of magnitude less than predicted on simple classical grounds and the relative decay of fast atom emission at different energies indicated the preferential loss of high energy ions. This observation led to the hypothesis that the electron temperature was being held at 20-30 eV by thermal conduction to an external heat sink, thus cooling the ions and consequently decreasing the ion-ion collision time. Computation using the program by Fisher and McNamara[16], which is based on the Fowler-Rankin model[17], supported this hypothesis and high-lighted the effect that cold electrons have on energy containment at high densities.

The experiments to be described differ from those reported at Novosibirsk in two main respects which have resulted in major changes of plasma behaviour. Firstly, the titanium getters have been used thus decreasing the background pressure and desorption from the vacuum walls. Secondly, a new divertor system considerably reduces

the amount of cold plasma which drifts into the trap after the initial filling stage. In addition several new diagnostic techniques have been used, namely:

1. an 8 mm interferometer for measuring line density;
2. a diamagnetic loop which is used during the confinement phase (c.f. ref. 15);
3. a neutral beam probe using either xenon or krypton for measuring electron temperature;
4. double electric probes for measuring fluctuating electric fields.

The present experiments show three new and important results. Firstly, there is a rapid loss of plasma resulting from the initial anisotropic velocity space distribution. Secondly, the overall plasma loss does not appear to be caused by Coulomb collisions between the ions and thirdly, electric potential fluctuations at ω_{ci}, the ion cyclotron frequency, have been observed.

2. THE APPARATUS

The confined plasma in the M.T.S.E. II magnetic well is established as follows; hydrogen plasma from a coaxial gun is channelled along an increasing magnetic guide field into the central vacuum chamber via an aperture limiter of 20 cm diameter (see Fig.1). By virtue of the increasing magnetic field the transverse ion velocity increases adiabatically so that approximately 20-30% of the plasma is reflected by the far magnetic mirror at the end of the central chamber; the remainder flows into the burial line. Before the reflected plasma can leave the central chamber the near mirror field, at the gun end of the central chamber, is established thus confining the plasma in a simple mirror system. At the same time a diverting system (described

in the next section) inhibits any further flow of plasma from the gun into the confined plasma. Finally the quadrupole stabilizing field is formed by passing current through the four longitudinal bars external to the plasma.

The magnetic mirrors, as well as the stabilizing field, are generated by current-carrying bars placed inside the central cylindrical vacuum chamber thus ensuring that the vacuum walls are remote from the confined plasma; the position of these bars is shown schematically in Fig.2. The mirror bars are 5·0 cm in diameter and the stabilizing bars are 7·6 cm in diameter; both sets of bars are inside glass tubes separating them from the vacuum. Mechanical movement of the stabilizing bars is reduced to a tolerable level by the four reflector bars shown in Fig.2. The induced currents which flow in these bars, via the vacuum tank and flanges, reduce the total magnetic force on the stabilizing bars[18].

The current in both sets of mirror bars and the stabilizing bars is supplied initially from 40 kV capacitor banks and subsequently maintained by several farads of electrolytic capacitors charged to between 200 V-350 V. The current in each mirror bar rises to 45 kA in 7 μsec or less and is held constant within 10% for 1 msec. The current in the stabilizing bars rises in 12 μsec and decays by between 10-20% in 1 msec depending upon the voltage of the electrolytic bank. The magnitude of this current is normally 125 kA per bar. The guide field and main B_z field are produced by coils external to the vacuum chamber; these fields rise in 0·14 sec to allow time for the magnetic flux to diffuse through the stainless steel walls of the vacuum chamber.

The configuration of the magnetic well, generated by the current-carrying bars and the external coils, is illustrated by the plots of

|B| shown in Figs.3a and 3b. The values of current and B_z chosen for these plots are those values normally used; they give a well depth of 1·3 at the last closed |B| surface and a longitudinal mirror ratio of 1·7 under the mirror bars. The effect of image currents in the tank walls and the reflector bars has not been taken into account but this effect is estimated to be small.

The main vacuum tank has an aluminium liner which was intended for liquid nitrogen cooling; in fact it has not been used. The entry and burial lines are ceramic tubes of 75 cm bore. The inside surfaces of these tubes and the main vacuum chamber can be coated with titanium evaporated from heated filaments. The system is pumped by two oil diffusion pumps which have a total pump speed of 2400 litres sec^{-1} and given a base pressure of 10^{-6} torr. When the titanium getters are used the base pressure drops to 2×10^{-7} torr. Further details of the construction of M.T.S.E. II can be found in ref.19.

3. EXPERIMENTAL RESULTS

The Injected Plasma

The injected plasma is produced by the coaxial gun used for the high density experiments on M.T.S.E. I[14]. The line density (i.e. $\int n d\ell$) of the injected plasma in the central chamber has been determined by measuring the attenuation of a beam of 4 keV potassium atoms[20] traversing the plasma horizontally, mid-way between the mirrors. In this method the attenuation caused by both electron impact and charge exchange are taken into account using the values of cross-section given in refs.20 and 21. The line density and maximum density have also been estimated using an 8 mm microwave interferometer with its path vertical at the mid-point between the mirrors. Both methods have

been cross-checked by using a moveable ion - collecting probe (as used for example in ref.22) to measure the magnitude of the plasma density and to derive the radial density profile. It was found that the maximum density occurs on, or near the axis and falls to zero in about 10 cm. The transverse energy per unit length, and hence β, of the injected plasma has been found by measuring the plasma diamagnetism.

The parameters of the injected plasma are given below. These parameters are only approximate owing to the irreproducibility of the gun operation and the integral nature of the measurements. It should also be noted that the parameters of that portion of the plasma which is reflected by the mirror fields, and thus trapped, differs in some degree from those of the injected plasma.

Plasma diameter	15-20 cm.
$\int n d\ell$	$1-2 \times 10^{14}$ cm^{-2}.
Maximum density	$\simeq 10^{13}$ cm^{-3}.
β	$\simeq 10\%$.
Mean ion energy	1-2 keV.

The plasma diameter, given by the above parameters, is approximately four ion gyro-radii ($4R_{ci}$ = 12 cm at 1·5 keV) which appears to be a consequence of the method of plasma injection[22]; this result applies to both the injected and trapped plasma.

Diversion of the Cold Plasma Produced by the Gun

In addition to the plasma which is trapped, the gun produces a similar quantity of slow-moving, low energy plasma which reaches the central chamber some 10-100 μsec later; if this cold plasma enters the trapping region and mixes with the trapped plasma it can

enhance the rate of energy loss and at the same time confuse the density measurement. In the M.T.S.E. I experiments[4,14] the cold plasma was successfully diverted and prevented from entering the trapping region by switching on a magnetic field in opposition to the guide field, thus establishing a cusp in the magnetic field lines between the gun and the trapping region; this divertor was supplemented by means of four current-carrying bars parallel to the machine axis, thus producing a quadrupole field immediately in front of the gun in addition to the cusp field. In practice, disrupting the field lines to divert plasma has not worked as well on M.T.S.E. II as it did on M.T.S.E. I, probably because of the increased diameter of the flight tube (75 cm instead of 30 cm); an alternative system is now used.

The new system for plasma diversion[23] relies on passing a current of approximately 10 kA through the slow plasma at right angles to the guide field so that the orthogonal $j \times B$ force drives the plasma into the flight tube wall before it can pass through the aperture limiter into the central chamber. The system is shown schematically in Fig.4. The effect of the two different divertors is demonstrated in Fig.5; this figure compares the line density, measured from the potassium beam attenuation, when plasma is injected into the guide field under different divertor conditions.

It should be noted that once the near mirror and the quadrupole stabilizing bars are switched on the resulting fields further inhibit the flow of plasma into the well.

The Initial Parameters of the Trapped Plasma

The parameters of the trapped plasma are taken to be those measured 20 μsec after plasma enters the trap, i.e. when all the

confining fields have been established. At this time the plasma diameter is essentially the same as that of the injected plasma, namely 15-20 cm. The initial ion density varies from shot to shot between 3×10^{12} cm^{-3} and 5×10^{12} cm^{-3} and the mean ion energy lies between 1 keV and 2 keV.

An important feature of the initial velocity distribution is demonstrated by Fig.6. The three curves of diamagnetism show the effect of altering the magnitude of the far mirror while the mirror near the gun is established normally at R = 1·7, and the stabilizing bars are not used. When no current flows in the far mirror the guide field has a mirror ratio of 1·08 (see field plot in Fig.1); hence the curve marked R = 1·08 shows the diamagnetism of untrapped plasma. In this case the diamagnetism after about 20 μsec is caused by plasma which has passed through the near mirror and consequently cannot be trapped unless the far mirror ratio exceeds 1·7. The increase of diamagnetism at the two higher values of R is caused by trapped plasma and gives an indication of the angular distribution of the ion velocities. The loss cone angles θ_c corresponding to the three mirror ratios are 49^o, 65^o and 74^o. It is apparent that there are more ions with velocity vectors lying between 49^o and 65^o than there are between 65^o and 90^o. Furthermore, because of the slight mirror effect in the guide field, there should be no ions at all between 74^o and 90^o; in addition the ion distribution should show a sharp boundary in velocity space at the loss cone angle (i.e. at $\theta = 49^o$). In short the majority of ions must have velocity vectors lying close to the loss cone angle θ_c (see insert in Fig.6). The effect of this distribution is to cause a rapid initial loss of plasma, as relatively small angle scattering causes ions to move into the loss cone and escape.

This initial loss is discussed in more detail in Section 4.

Fig.7 shows the initial effect on diamagnetism of applying the stabilizing field. For the first 70 μsec the mirror diamagnetism exceeds that of the well. This excess is equal to the diamagnetism shown in Fig.6 for the case of R = 1.08 and can be attributed to plasma entering the trap after the fields have been established. In the mirror case this plasma flows into the trap and through the diamagnetic loop but, in the well case, it is diverted sideways and misses the loop. After 80 μsec the well diamagnetism exceeds that of the simple mirror because the latter is showing signs of gross instability at this time. In the mirror case small discontinuities in diamagnetism are first observed at 60 ± 27 μsec (standard deviation of 23 observations).

Comparison between the Magnetic Well and Simple Mirror

The oscillograms in Fig.8 illustrate the effect of the stabilizing bars on plasma behaviour. All four pairs of oscillograms show that, in the simple mirror case, the plasma is grossly unstable inside 100 μsec. At this time the diamagnetic signal shows the first of two discontinuities while the microwave interferometer signal fluctuates and behaves erratically compared with the well case.

The oscillogram marked 'Xe beam' shows the amplitude of a pulsed beam of 8 keV xenon atoms after it has traversed the plasma horizontally. This beam is attenuated by both electron impact ionization and charge exchange with the contained hydrogen ions. Once the plasma line density (measured by the 8 mm interferometer) is known the electron temperature can be deduced from the beam attenuation. This method of measuring T_e has been described by Hughes[24]. Krypton as well as xenon has been used; the relevant cross-sections are given in

refs.25, 26 and 27. The base line shift of the xenon oscillogram occurs because the neutral beam detector is sensitive to light. It is seen that, in the simple mirror case, a burst of light is emitted from the plasma soon after it becomes unstable.

The oscillograms showing the flux of 1·6 keV atoms from the plasma were obtained with the detector[28] set at an angle of 68° to the machine axis. In the mirror case the fluctuating atom flux also indicates a gross instability; in the well case the atom flux shows a smooth decay and typically lasts up to 1·7 msec.

The line density measured by the potassium beam also showed discontinuities which correlated with those in diamagnetism for the mirror case. When the stabilizing bars were used the line densities measured by the potassium beam[20] and the microwave interferometer decayed smoothly and agreed within experimental error. The line density was also measured using hydrogen in conjunction with the krypton beam[24]; although the hydrogen attenuation was very small, making accurate measurement impossible, the line density obtained was consistent with the other measurements.

Plasma Behaviour in the Magnetic Well

Fig.9 shows the behaviour of the plasma density n, the mean ion energy W_i and the electron temperature T_e, obtained from the oscillograms in Fig.8. The table in Fig.9 compares T_e measured by the xenon beam with that deduced from the measured decay of W_i on the assumption that the ion-electron collisions are classical. The details of the method used are described in Section 4. Although density measurements continue to 1 msec, and the fast atom emission to 1·7 msec, the diamagnetism is too small for accurate measurement after 300–400 μsec, therefore the behaviour of the mean ion energy is uncertain beyond this time; the value of T_e is also uncertain

beyond this time. The initial drop in density shown in Fig.9 is typical. The average decay of ion energy at 200 μsec is $2{\cdot}6 \pm 1{\cdot}6$ eV μsec^{-1} (standard deviations of 20 observations), and the average value of T_e measured by the Xe and Kr beams is $15{\cdot}1 \pm 5{\cdot}8$ eV (standard deviation of 10 observations); swept Langmuir probe measurements are consistent with this temperature.

The behaviour of fast atom emission at three angular positions is shown in Fig.10. Although the initial behaviour of amplitude depends on position and energy the fast atom emission at 1 keV, 1·6 keV and 4 keV always shows approximately the same smooth decay after about 400 μsec, although the time at which emission ceases does depend on energy. The 1·6 keV emission ceases at $1{\cdot}6 \pm 0{\cdot}2$ msec (standard deviation of 15 observations) while 4 keV emission ceases at $1{\cdot}3 \pm 0{\cdot}1$ msec (standard deviation of 17 observations). The increase in the duration of fast atom emission compared with that reported at Novosibirsk[15] is mainly the result of using the titanium getters.

The original attempt[15] to find high frequency potential fluctuations in M.T.S.E. II used a single capacitative probe and was made before the titanium getters and the new divertor were used; these measurements failed to show any r.f. activity. Later measurements, made after gettering, used a double probe of the type described by Ashby and Paton[29]; these measurements showed two short bursts of noise, of approximately 5 μsec duration, occurring as the near mirror bars and stabilizing bars were energized. More significantly this probe also detected fluctuating electric fields of 1 V cm^{-1} or less, at a radius of 20 cm, which persisted for the first few hundred microseconds. At the time these fluctuating fields were dismissed as

being too small to account for the rapid initial plasma loss[30].

Recently a double probe technique has been used to measure potential fluctuations across the plasma diameter. Fig.11 shows details of this technique and the results obtained. The amplitude of the fluctuations is greater than 100 V initially and decreases progressively to less than 10 V. The highest discernible frequency is the ion-cyclotron frequency and the r.f. envelope shows slight modulation of about 10 μsec period, which roughly corresponds to the ion transit time between mirrors. Although the probes are at 15 cm radius, and nominally out of the plasma, there is a tenuous plasma ($n \simeq 10^{10}$ cm^{-3}) at this radius and the presence of the probes reduced the time of fast atom emission by a factor of approximately two. This measurement of r.f. potential across the plasma diameter, in conjunction with the earlier measurement of electric field, indicates that there is probably no more than one complete wavelength around the plasma circumference.

All the measurements described in the section above were made using a well depth which started at 1·3 and dropped to about 1·05 in a millisecond. Less complete measurements, in which the well depth decayed to 1·15, showed no noticeable difference. Increasing the well depth to 1·45 also failed to alter the plasma behaviour.

4. COMPARISON BETWEEN THEORY AND EXPERIMENT

Derivation of n and W_j from Line Density and Diamagnetism

To compare theory and experiment the relationships between the measured parameters and those used in the theory must be known; these relationships are more complicated than might be expected at first glance. The main measured plasma parameters are line density and diamagnetism (hereafter referred to as L and D respectively) but plasma density

n and mean ion energy W_i are used in the theory and experiment. The relationship between these two pairs of parameters depends upon the radial variation of density and as the plasma radius is not large compared with an ion gyro-radius, some averaging procedure must be used to give the mean plasma density sampled by the typical ion as it gyrates. The method used to relate the measured and the plasma parameters is outline below.

The radial dependence of density is not known with any certainty so three different profiles have been considered; these are specified below in terms of the maximum plasma density n_o and the maximum plasma radius r_o.

(a) A square distribution in which $n = n_o$ from $r = o$ to $r = r_o$.

(b) A parabolic distribution given by $n = n_o \{1 - (r/r_o)^2\}$.

(c) A triangular distribution given by $n = n_o (1 - r/r_o)$.

Whenever a plasma parameter depends upon the density, profile (b) is used but the effect of using the two extreme profiles (a) and (c) is also quoted to illustrate the degree to which the parameter is sensitive to the assumed profile.

A crude attempt is made to average n over a typical ion orbit; this is done analytically for the three profiles by assuming that a typical ion gyrates through the axis and the plasma edge (i.e. $2 R_{ci} = r_o$). The average density used is either the mean or the root mean square depending upon which is most appropriate. The derived quantities are expressed in terms of L, D and r_o to show their dependence upon the measured quantities. All the numerical values presented are for $r_o = 10$ cm.

The plasma parameters in the previous sections were derived in

the following way. The density in Fig.9 is the R.M.S. value and is given by

$$n = K_1 \, L/r_o \ , \qquad \ldots (1)$$

where the value of the constant K_1 changes by + 9% and - 6% when the triangular and square density profiles respectively are used instead of the parabolic distribution. Similarly the mean ion energy is given by

$$W_i = K_2 D/(L r_o) \ , \qquad \ldots (2)$$

where K_2 varies by - 25% (square profile) and + 13% (triangular profile). Stictly speaking W_i is the mean ion energy associated with transverse ion motion alone but the difference between this value and the total ion energy is only about 10% or less for the mirror ratios used.

Electron Temperature and Ion Cooling

Spitzer[31] gives an expression for the equipartition time caused by Coulomb collisions; this equipartition time describes the rate of energy transfer from hot ions to cold electrons and is used to derive the electron temperature T_e(cooling) which would account for the measured decay of mean ion energy. The following equation is used:

$$\frac{dW_i}{dt} = - \frac{8(2\pi)^{\frac{1}{2}} n e^4}{3(KT_e)^{3/2}} \frac{m_e^{\frac{1}{2}}}{m_i} W_i \ln\Lambda \ ; \qquad \ldots (3)$$

hence

$$T_e^{3/2}(\text{cooling}) = - K_3 \, D/\{r_o \frac{d}{dt}(\frac{D}{L})\} \ , \qquad \ldots (4)$$

where the constant K_3 varies by + 33% (square profile) and - 4% (triangular profile). The mean value of n is used and r_o and the density profile are assumed to be constant.

The electron temperature derived from Eq. (4) compares with that measured from the attenuation of the Kr and Xe beams as follows:

$$\frac{T_e(Kr)}{T_e(cooling)} = 1{\cdot}9 \pm 0{\cdot}7 \text{ (standard deviation of 23 observations)},$$

$$\frac{T_e(Xe)}{T_e(cooling)} = 2{\cdot}8 \pm 0{\cdot}9 \text{ (standard deviation of 13 observations)}.$$

The measured value of T_e agrees with $T_e(cooling)$ to within a factor of three or four and hence the ion-electron coupling is consistent with Coulomb collisions after making allowance for experimental inaccuracies and uncertainties in the assumptions. The question arises why is T_e slowly decreasing insteady of increasing? In the M.T.S.E. II Novosibirsk paper[16] it was postulated that cold plasma external to the contained plasma cooled the trapped electrons by thermal conductivity. An external plasma with T_e = 2 eV and in good thermal contact with a heat sink, such as the vacuum chamber, would produce the observed dW_i/dt if its density exceeded about 10% of the trapped density; this percentage compares with about 3% which will result from escaping plasma as it streams through the mirrors. The escaping electrons will also cool the plasma because their energy exceeds 3/2 kT_e as a result of the positive plasma potential caused by ambipolar diffusion; however, this effect is nearly two orders of magnitude too small to account for the observed dW_i/dt. The cooling effect of charge exchange with background neutrals is also too small to account for the observed decay of ion energy.

The Decay of Plasma Density

Several computer programs exist for predicting the plasma decay in mirror machines; they range in complexity from the Fowler-Rankin[17] type, which takes into account the changing energy distribution of

the trapped particles and electric potentials, to the program by Killeen and Marx[32] which also allows for spatial variation along the field lines and a changing ion velocity space distribution. Although these programs are invaluable for determining the feasibility of mirror machines as fusion reactors, they are not altogether ideal for checking experimental results; difficulties can arise because of expense and running time, the number of initial parameters which are not known accurately, the number of experimental results and the effect of radial variations. The approach in this paper is to simplify the equations used and to compare the magnitude and functional dependence of dn/dt with experiment.

The measurement of T_e shows that the effect of electric potentials is small and can be ignored since $T_e \ll W_i$[33]. The averaging technique used to allow for the radial variation of density has already been described in the previous section. The differential equation describing the loss rate is of the form

$$\frac{dn}{dt} = \frac{n}{\tau_{ii} F(R,f)} \quad , \qquad \ldots (5)$$

where τ_{ii} is the ion-ion collision time given by Spitzer[31] with $3/2kT_i = W_i$, i.e.

$$\tau_{ii} = \frac{(2m_i)^{\frac{1}{2}} W_i^{\frac{3}{2}}}{4\pi e^4 n \cdot \ln\Lambda} \quad . \qquad \ldots (6)$$

The function $F(R,f)$ describes the effect of the mirror ratio and the function f, which in turn describes the distribution of the ions in velocity space (see Eq.9). The function F approximates to $\log_{10} R$ once the angular distribution is steady[34,35] and the effect of ion cooling by cold electrons can be estimated by solving Eqs.(3) and (5) numerically. The accuracy of this method has been estimated by comparing $\tau_{ii} \log_{10} R$ with the equivalent time $n/(dn/dt)$ obtained

from the Fisher-McNamara program[16]; in every case the two times were within a factor two and the variation with time was even smaller.

The effect of the initial angular distribution* of the injected plasma (see Fig.6) has been estimated from the diffusion equation

$$\frac{\partial f}{\partial t} = K \frac{\partial^2 f}{\partial \theta^2} \qquad \ldots (7)$$

and

$$n = \int_{\theta_c}^{\pi/2} f d\theta \ , \qquad \ldots (8)$$

where f is the distribution function of the ions,

i.e. $$dn = f d\theta = h(t)\ g(\theta, t)\ d\theta \qquad \ldots (9)$$

and the diffusion coefficient K is given by

$$K = 4(\pi/2 - \theta_c)^2/\tau_{ii}\pi^2 \log_{10} R \ . \qquad \ldots (10)$$

Equations (3), (6), (7), (8) and (9) are rapidly solved numerically for any initial angular distribution f, by assuming the ions are mono energetic. (The diffusion equation (7) has been simplified by working in Cartesian co-ordinates rather than spherical co-ordinates as the results are more general and this approximation is justified for $R \leqslant 1{\cdot}7$).

The effect of different initial angular distributions is shown in Fig.12 and the effect of ion cooling by cold electrons is shown in Fig.13. The curves in Fig.12 are plotted against a normalized time scale as they are general, in constrast to those in Fig.13

*BenDaniel and Allis[36] also consider the effect of different initial angular distributions but with distributions peaked around $\theta = 90^o$ and not $\theta = \theta_c$.

where the cooling equation has been used. To get a real time scale in Fig.13 the mirror ratio is taken as 1·7. It can be argued that the well depth of 1·3–1·1 should be used instead. However, the full mirror ratio appears more appropriate on two counts. Firstly, Fig.7 shows that the diamagnetism is nearly the same for well and mirror in the first 100 μsec; therefore during this time R = 1·7 must be correct. Secondly, if the well depth were the deciding factor, the two fast atom detectors at 68^{o} (see Fig.10) would be looking inside the loss cone once the well depth had dropped below 1·16 and consequently would show an abrupt decrease in signal at late times; this does not occur.

Figs.12 and 13 demonstrate the wide variation in the behaviour of density decay which can occur under different initial conditions. After making allowance for the uncertainty of the initial conditions, the density profile, the plasma radius and the theoretical assumptions, it is not obvious whether or not the experimental points in Fig.13 represent a tolerable fit with theory. It should be noted that these points are optimistic as experimentally the mean initial conditions are $n_o = 3{\cdot}7 \times 10^{12}$ cm^{-3} and $W_i = 1{\cdot}3$ keV, which differ slightly from the theoretical initial conditions of $n_o = 5 \times 10^{12}$ cm^{-3} and $W_i = 1.0$ keV. The technique for deciding whether the results do agree with theory is described next.

From Eq.5 the quantity $(\tau/n)\ dn/dt$ should be unity for $\tau = \tau_{ii}F(R,f)$. Once the initial rapid decay of density is over and the angular distribution is steady $F \rightarrow \log_{10}R$. Hence

$$\frac{\tau}{n} \cdot \frac{dn}{dt} \rightarrow \frac{\tau_{ii} \log_{10}R}{n} \cdot \frac{dn}{dt} = K_4 \frac{D^{3/2}}{r_o^{1/2} L^{7/2}} \frac{dL}{dt} , \qquad \ldots (11)$$

where the value of the constant K_4 varies by - 47% (square profile) and + 41% (triangular profile) depending upon the assumed radial

variation of density. In Eq.(11) the R.M.S. value of n is used and r_o is assumed to be constant.

On the assumption that the velocity space distribution is steady at 200 μsec, $(\tau/n)\ dn/dt$ is evaluated at this time for a series of shots giving

$$\frac{\tau}{n}\frac{dn}{dt} \simeq \frac{\tau_{ii}\log_{10}R}{n} \cdot \frac{dn}{dt} = 32 \pm 22 \text{ (standard deviation of 26 observations).}$$

This result demonstrates two points; firstly $(\tau/n)\ dn/dt$ is about one order of magnitude larger than can reasonably be explained; secondly, the large standard deviation shows that this parameter does not remain constant from one shot to another. In short the effective ion-ion scattering time τ, which causes plasma loss, is much smaller than τ_{ii} and has a different fuctional dependence. The behaviour of density with time suggest that this effective ion-ion scattering time remains constant; this fact is shown by evaluating $(1/n)\ (dn/dt)$ for the data used previously giving:

$$\frac{1}{n} \cdot \frac{dn}{dt} = \frac{1}{L} \cdot \frac{dL}{dt} = (4{\cdot}71 \pm 0{\cdot}95) \times 10^3 \text{sec}^{-1} \ .$$

Figs.14 and 15 show, in a more convincing fashion, the functional dependence of τ. The parameter $(\tau/n)\ (dn/dt)$ is plotted against n/n_o under two different assumptions namely, τ = 250 μsec and $\tau = \tau_{ii}\log_{10}R$. The curves in Fig.14 show $F/\log_{10}R$ against n/n_o for three initial angular distributions of velocity; by plotting in this way the theoretical curves are general and independent of the behaviour of τ. When τ is assumed to be constant, there is good agreement with theory from start until 99% of the plasma has escaped. In contrast, when we assume $\tau = \tau_{ii}\log_{10}R$ the experimental observations differ from theory on three counts, namely:

1. the amplitude of $(\tau/n)\ dn/dt)$ is a factor 40 too large;
2. the experimental points do not show the initial

drop which results from the angular distribution;

3. the standard deviations of the experimental points show that $(\tau/n)\ (dn/dt)$ is not a constant.

Plasma loss resulting from charge exchange should not affect the measured decay rate and the above results. Unless the neutral background pressure rises during a shot, charge exchange losses only become comparable to the plasma loss rate after 1 msec when $n < 10^{10}$ cm^{-3}. The fast atom emission signals give no indication of a significant increase in background pressure.

Fast Atom Emission

The measurement of fast atom emission, illustrated in Fig.10, also suggests that the plasma loss is not caused by Coulomb collisions. The three detectors, which look at the same portion of the trapped plasma from different angles, always give signals which differ initially but after the first 400-500 μsec they show the same smooth decay. The shape of the signals should differ until the angular distribution of ion velocities is steady; Fig.14 shows that this happens at about 400 μsec which agrees well with the fast atom emission measurement.

Non-classical ion-ion interaction is suggested by the fact that the 1 keV and 4 keV signals both decay smoothly after 400-500 μsec (see Fig.10); if the collision time showed the $W_i^{3/2}$ dependence, characteristic of Coulomb collisions, then the 4 keV ions would take six times longer than the 1 keV ions to assume a steady angular distribution.

The High Frequency Electric Fields

The observations made on the fluctuating electric potentials are insufficient to identify their cause but the simple order of magnitude

calculation outlined below shows that the measured electric field, of approximately 1 V cm^{-1} could account for the observed loss rate.

The fractional change in ion energy, produced by the electric field E in the one gyro-period is given by

$$\frac{\Delta W_i}{W_i} \simeq \frac{\pi}{v_i} \cdot \frac{E}{B} \quad , \qquad \ldots (12)$$

where v_i is the ion velocity and the field E is assumed to act for a quarter of a period. The number of ion gyrations occurring in one e-folding time τ, which describes the plasma loss rate, is

$$N = \omega_{ci}\tau/2\pi \quad . \qquad \ldots (13)$$

To determine the average change in ion energy $\overline{\Delta W_i}$ during an e-folding time some assumption must be made about the degree of correlation between the r.f. field and the ion motion. If the phase between the field and a typical ion remains unchanged for a fraction α of the N cycles before changing to a new arbitrary phase for the next αN cycles then

$$\overline{\Delta W_i}/W_i \simeq \frac{\pi}{v_i} \cdot \frac{E}{B} \cdot N\alpha^{\frac{1}{2}} \quad . \qquad \ldots (14)$$

Substitution of experimental values into Eq.(14) gives

$$\overline{\Delta W_i}/W_i \simeq 3\alpha^{\frac{1}{2}} \quad . \qquad \ldots (15)$$

For a substantial number of ions to be scattered into the loss cone $\overline{\Delta W_i} \simeq W_i$ i.e. $\alpha \simeq 0{\cdot}1$. If the observed r.f. fluctuations are to account for the observed loss rate then there must be some degree of correlation; if, on average the phase between the typical ion and the field takes about one hundred cycles to change (i.e. $\sim$ 25 μsec) then the observed loss rate would be consistent with the observed electric field fluctuations.

5. DISCUSSION

The results presented differ considerably from those described at Novosibirsk; the differences all reflect a major reduction in the quantity of cold plasma which flows, from the injection line into the trap, during the first few hundred microseconds. At the time of Novosibirsk this cold plasma dominated the line density measurements thus obscuring the behaviour of the trapped plasma. Although the presence of cold plasma was recognised at the time of Novosibirsk its effect on the measurement of line density was not fully appreciated.

In Section 4 it was concluded that the ion scattering time was an order of magnitude greater than classical and did not have the functional dependence appropriate to Coulomb collisions. The procedure used to compare experiment with theory can be criticised on several grounds (e.g. it ignores axial variations and does not take into account the changing energy distributions). However, it makes possible the rapid comparison of a large number of experimental results when the plasma parameters vary from day to day and enables an explicit estimate to be made of the effect of experimental uncertainty in parameters such as radius and density profile; without this detailed analysis and the variety of diagnostics used it would not be obvious that the loss rate is an order of magnitude greater than classical.

The determination of electron temperatures from the observed ion cooling rate is not very accurate and the fact that T_e(cooling) equals the measured value of T_e to within a factor of three or four is certainly consistent with classical interaction between the ions and electrons. However, the loss in ion energy due to classical cooling by cold electrons is comparable to the energy loss due to escaping ions, despite the anomalously high loss rate; hence even if the

microinstability, causing the potential fluctuation, does transfer energy between the ions and electrons it is unlikely that there would be a measurable change in the ion cooling rate.

It has not been possible to identify the instability responsible for the r.f. fluctuations and presumably the plasma loss. The drift cyclotron instability[7] theoretically can occur; this instability couples the ions and electrons but, as we have seen above, the resulting increases in energy transfer rate between ions and electrons would probably be unnoticed. The plasma density appears to be too high for the 'modified negative mass instability'[9] although this instability might be encouraged by the unusual ion distribution brought about by the filling method. A final possibility is an ion-ion instability due to a 'double humped' ion energy distribution i.e. hot ions streaming through cold ions[12].

6. CONCLUSIONS

The plasma loss mechanism in M.T.S.E. II is approximately one order of magnitude too large to be explained by Coulomb collisions. The loss is characterized by an effective ion scattering time of about 250 μsec which is approximately constant during the first millisecond as β drops from an initial value of ~ 10%. The rapid initial drop in density is attributed to the method of plasma formation which results in a velocity space distribution peaked near the loss cone angle. The anomalous plasma loss rate appears to be associated with an electrical field of ~ 1 V cm^{-1} fluctuating at frequencies close to ω_{ci}; the instability causing these fluctuations has not been indentified.

The range of diagnostics and the detailed analysis used demonstrate the difficulty of distinguishing between classical and non-classical

behaviour when the loss rate is within an order of magnitude of the classical value.

7. ACKNOWLEDGEMENTS

The authors wish to thank Drs R.S. Pease and R.J. Bickerton for their stimulating interest and to express their sincere appreciation of the invaluable assistance given by R.A. Boone, B.D. Cooper, R.G. Montague, G.O.R. Naylor and A. Travis in obtaining the experimental results. The efforts of the engineering team, headed by K.M. Plummer, in building, maintaining and modifying M.T.S.E. II is gratefully acknowledged.

REFERENCES

1. GOTT, Y.B., IOFFE, M.S. and TELKOVSKY, V.G., Proc. 1st Conf. Plasma Physics & Controlled Fusion, Salzburg (1961). Nucl. Fusion Suppl. 3 (1962) 1045.

2. BIGUET, A., BLANC, P., GRAVIER, R., LECOUSTEY, P., LUC, H., RENAUD, C., TACHON, J., VERON, D. and ZANFAGNA, B., Compt. Rend. Acad. Sci. 259 (1964), 1040.

3. DAMM, C.C., FOOTE, J.H., FUTCH, A.H., GARDNER, A.L. and POST, R.F., Phys. Rev. Lett. 13 (1964), 464.

4. FRANCIS, G., MASON, D.W., and HILL, J.W. Nature 203 (1964) 623.

5. TAYLOR, J.B., Phys. Fluids 6 (1963), 1529.

6. TAYLOR, J.B. Phys. Fluids 7 (1964), 767.

7. ROSENBLUTH, M.N. and POST, R.F. Phys. Fluids 8 (1965) 547.

8. HALL, L.S., HECKROTTE, W. and KAMMASH, T. Phys. Rev. 139A (1965) 1117.

9. CALLEN, J.D. and HORTON, C.W. Phys. Fluids 13 (1970) 154.

10. DAMM, C.C., FOOTE, J.H., FUTCH, A.H., HUNT, A.L., MOSES, K., POST, R.F. and TAYLOR, J.B. Phys. Rev. Lett. 24 (1970) 495.

11. CORDEY, J.G., KUO-PETRAVIC, G., MURPHY, E.G., PETRAVIC, M., SWEETMAN, D.R. and THOMPSON, E. Proc. 3rd Conf. Plasma Physics & Controlled Fusion, Novosibirsk (1968) p.267. 2 (1969) 267.

12. COENSGEN, F.H., CUMMINS, W.F., ELLIS, R.E. and NEXSEN, W.E. Proc. 3rd Conf. Plasma Physics & Controlled Fusion, Novosibirsk, (1968) 2 (1969) 225.

13. TAYLOR, J.B. and HASTIE, R.J. Phys. Fluids 8 (1965), 323.

14. FRANCIS, G., HILL, J.W. and MASON, D.W. Proc. 2nd Conf. Plasma Physics & Controlled Fusion, Culham (1965) 1 (1966) 53.

15. FRANCIS, G., HILL, J.W., McNAMARA, B. and MASON, D.W., Proc. 3rd Conf. Plasma Physics & Controlled Fusion, Novosibirsk. 2 (1969) 239.

16. FISHER, D.L., McNAMARA, B. and MASON, D.W. Proc. Int. Conf. on Plasma Confined in Open-Ended Geometry, Gatlinburg, (1967) 280.

17. FOWLER, T.K. and RANKIN, M., Plasma Phys. (J. Nucl. Energy Part C), 4 (1962). 311.

18. FRANCIS, G., SMART, D.L. and MEDFORD, R.D. Symp. on Eng. Problems of Controlled Thermonuclear Research Gatlinburg, (1966).

19. PLUMMER, K.M. and SKELTON, D.E. 5th Symposium on Fusion Technology, Oxford Paper 65, (1968).

20. HILL, J.W., MASON, D.W. and TRAVIS, A. Report CLM-R 68. (1967).

21. GARCIA, J.D. and GERJUOY, E. Phys. Rev. 165 (1968), 72.

22. ASHBY, D.E.T.F. and AVIS, B.E. Plasma Phys. (J. Nucl. Energy Pt.C), 8 (1966) 1.

23. HUGHES, M.H. and MONTAGUE, R.G. To be published.

24. RAPP, D. and ENGLANDER-GOLDEN, P. J., Chem. Phys. 43 (1965), 1464.

25. STEDEFORD, J.B.H. and HASTED, J.B. Proc. Roy Soc. (Lond.) A.227 (1955) 466.

26. KOOPMAN, D.W. Phys. Rev. 154 (1967). 79.

27. HUGHES, M.H., HILL, J.W. and COOPER, B.D. Proc. 3rd European Conf. on Controlled Fusion and Plasma Phys. Utrecht (1969) p.13.

28. MASON, D.W. and SCHOFIELD, J.M.S. Report CLM-R 49, (1966).

29. ASHBY, D.E.T.F. and PATON, A. Plasma Phys. 9 (1967), 359.

30. ASHBY, D.E.T.F., BYDDER, E.L., HILL, J.W., HUGHES, M.H. and MASON, D.W. Bull Amer. Phys. Soc. series II, 14 (1969), 1054.

31. SPITZER, L. Physics of Fully Ionized Gases, Interscience Pub. Inc. (1956).

32. KILLEEN, J. and MARX, K.D. To be published in Methods in Computational Physics, Acad. Press.

33. BENDANIEL, D.J. Plasma Phys. (J. Nucl Energy Pt.C) 3 (1961) 235.

34. JUDD, D., McDONALD, W. and ROSENBLUTH, M., U.S.A.E.C. Report WASH-289 (1955), 158.

35. BUDKER, G.I. Plasma Physics and the Problems of Controlled Thermonuclear Reactions. Pergamon Press. III (1959), 1.

36. BENDANIEL, D.J. and ALLIS, W.P. Plasma Phys. (J. Nucl. Energy Pt. C) 4 (1962) 31.

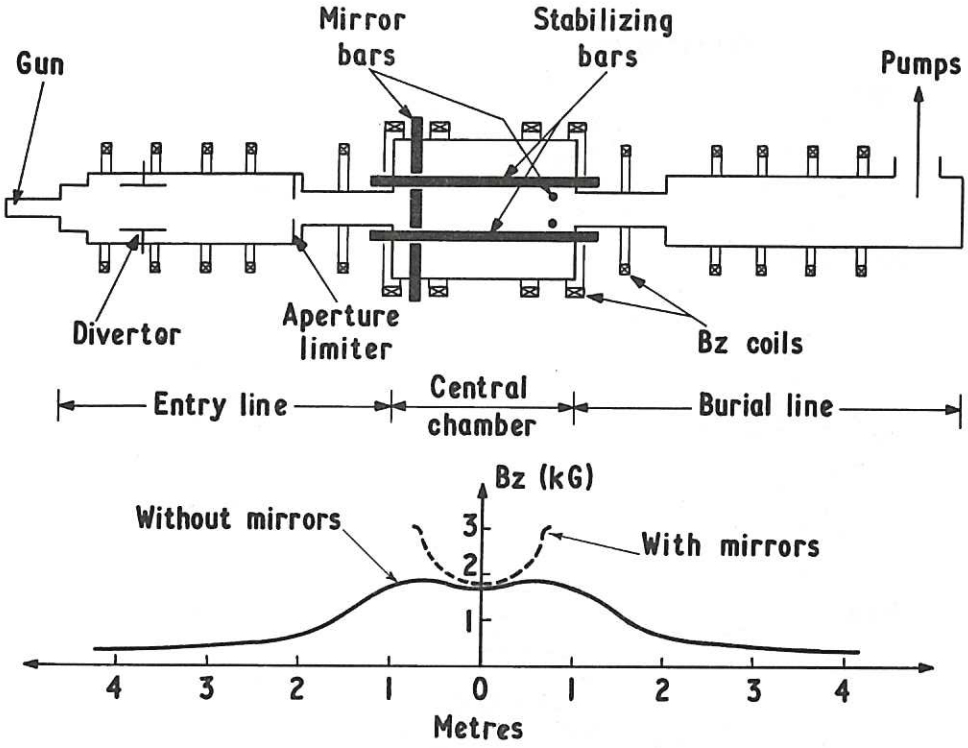

Fig.1 (CLM-P 245)
Schematic diagram showing the layout of M.T.S.E. II and the variation with distance of B_z with and without the mirrors. The distance scale refers to both the field distribution and the schematic diagram.

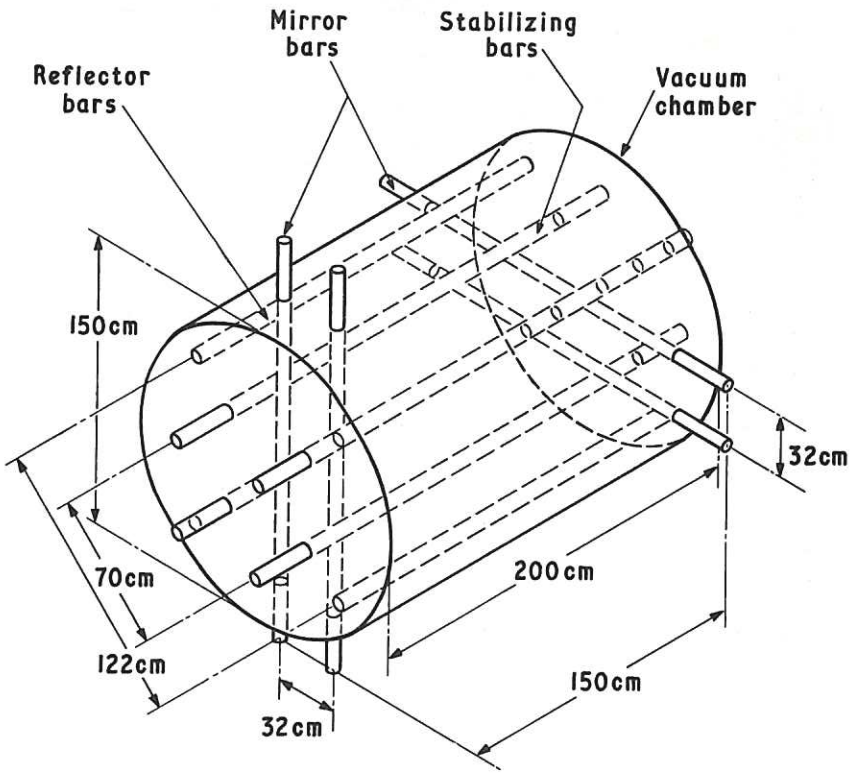

Fig.2 (CLM-P 245)
Schematic diagram showing the configuration of the mirror bars, stabilising bars and reflector bars within the main vacuum chamber.

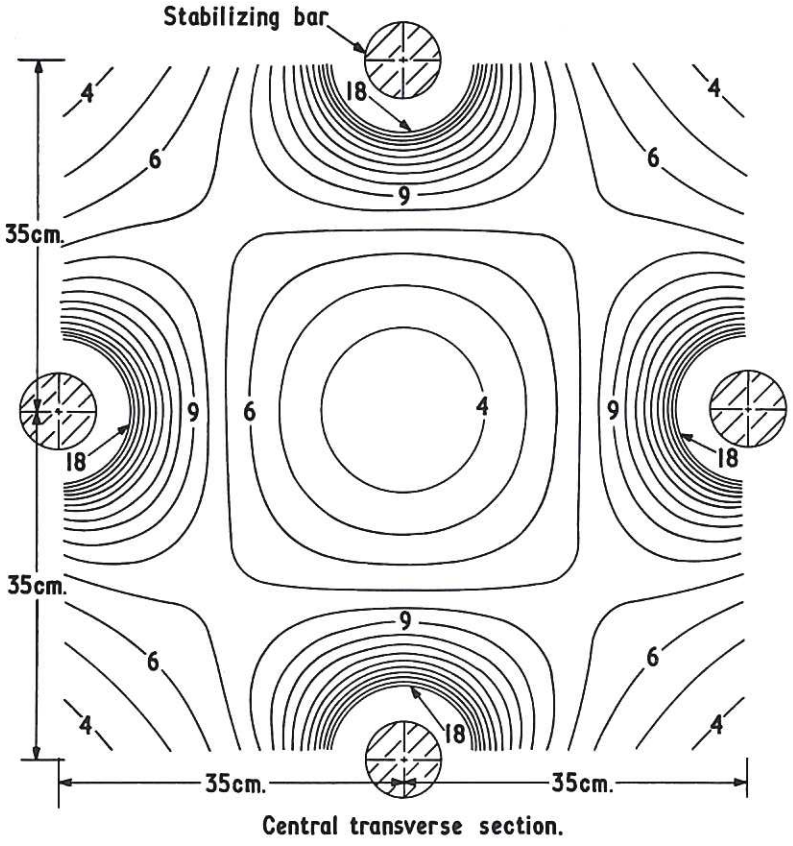

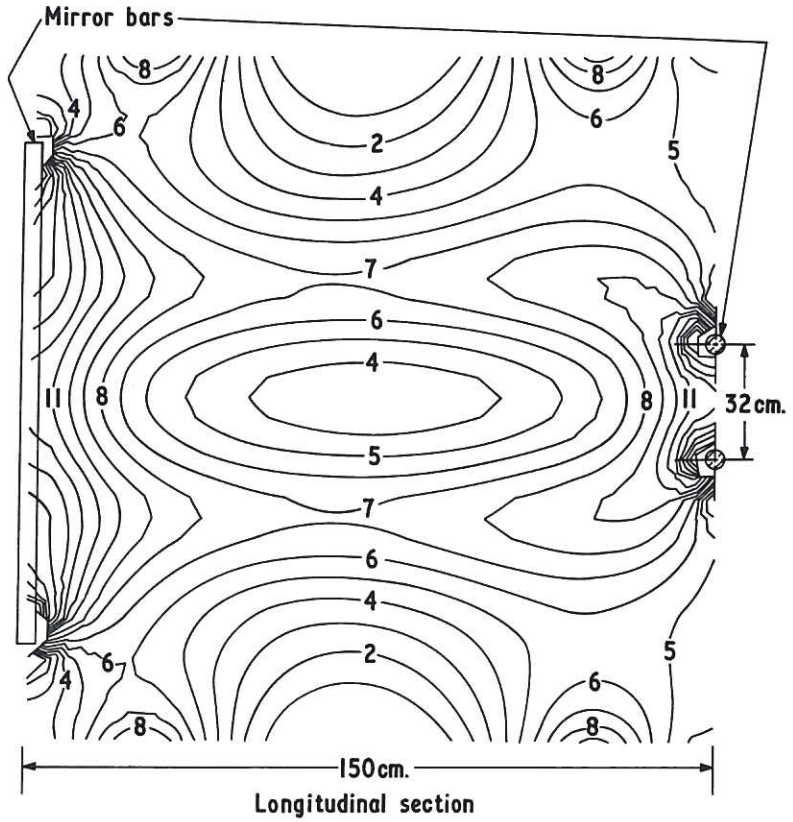

Figs.3a and 3b (CLM-P 245)

Plots of |B| for: mirror bar current = 45 kA; stabilising bar current 125 kA; guide field 770A. The field strength along any contour is given by |B| = (1·3 + 0·15n) KG where n is the number associated with the contour.

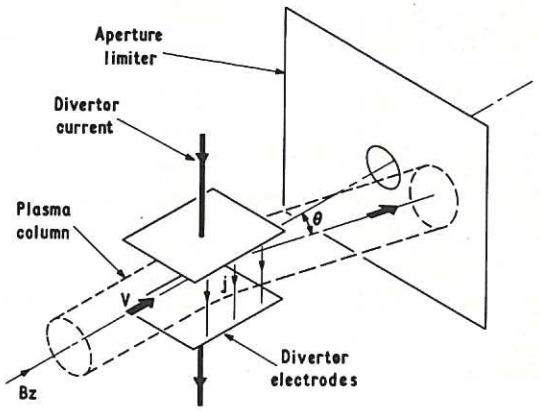

Fig.4 (CLM-P245)
Schematic showing the j × B divertor used to prevent slow plasma, from the gun, entering the magnetic well.

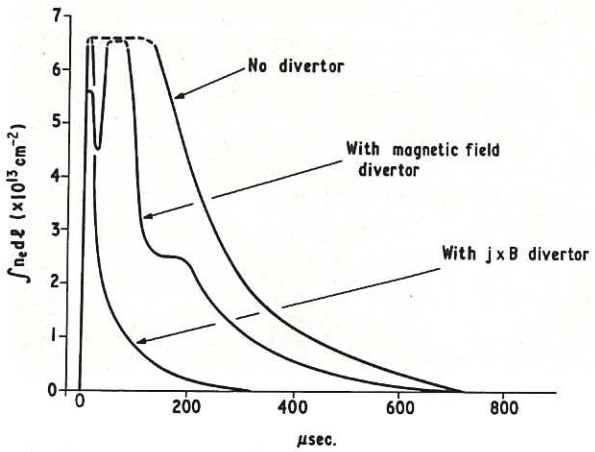

Fig.5 (CLM-P245)
Line density against time when plasma is injected into the guide field with no mirror fields. The effect of the j × B divertor is compared with that of the magnetic divertor and no divertor.

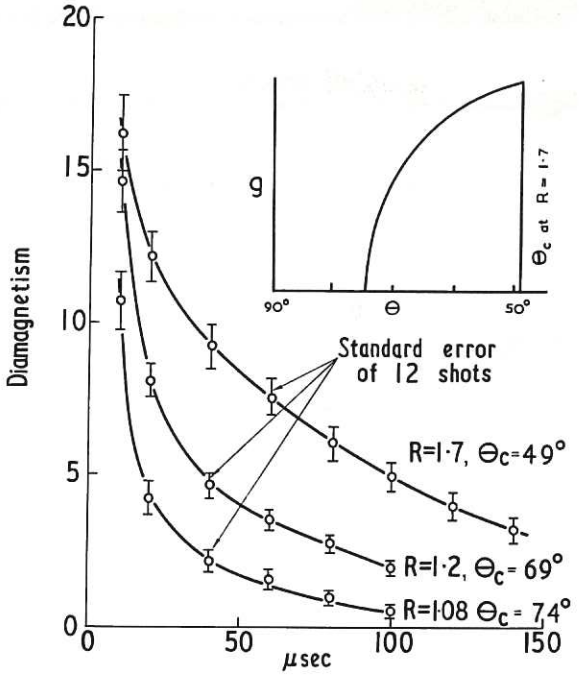

Fig.6 (CLM-P245)
Curves of diamagnetism showing the effect of altering the mirror ratio R of the far mirror and hence θ_c the loss cone angle. In the case of R = 1·08 the rear mirror is not used and the mirror ratio is produced by the guide field alone (see Fig.1). The insert illustrates the form of the initial angular distribution of the ions for R = 1·7.

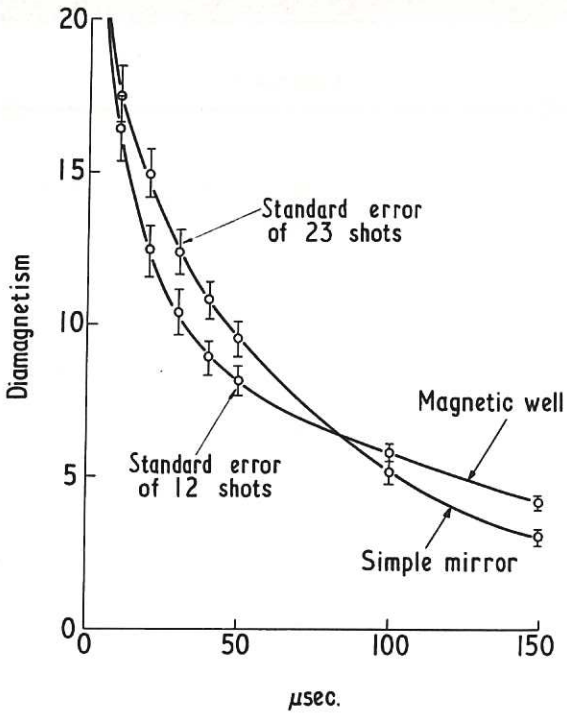

Fig.7 (CLM-P245)
Curves comparing the initial diamagnetism of simple mirror and magnetic well geometries.

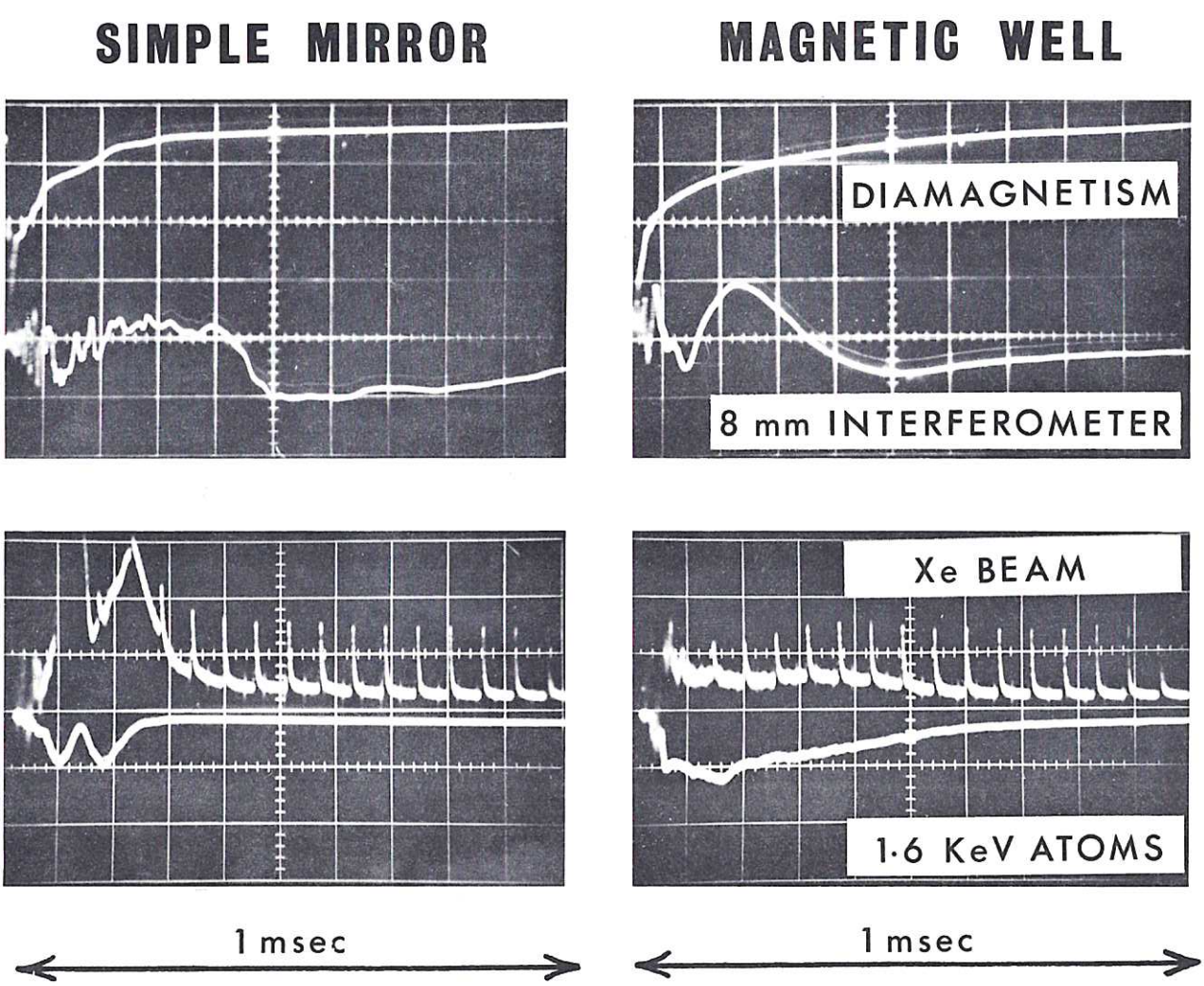

Fig.8 (CLM-P 245)
Oscillograms illustrating the effect of the stabilising bars. The trace marked 'Xe beam' shows the amplitude of a pulsed beam of Xe atoms, the base line shift is due to light emitted from the plasma. The trace marked 1·6 keV atoms shows fast atom flux at an angle of 68° to the machine axis.

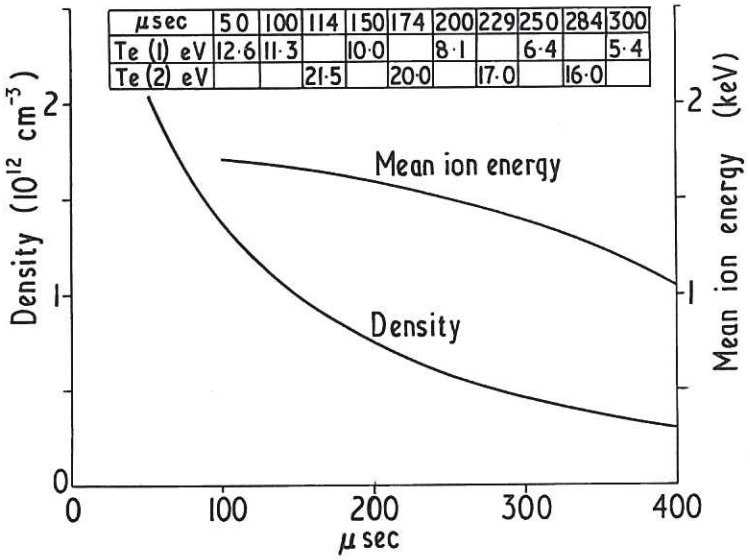

Fig.9 (CLM-P 245)
Typical behaviour of plasma parameters in the magnetic well. These results are obtained from the oscillograms in Fig.8. $T_e(1)$ refers to the electron temperature deduced from dW_i/dt while $T_e(2)$ refers to that measured from the xenon beam attenuation.

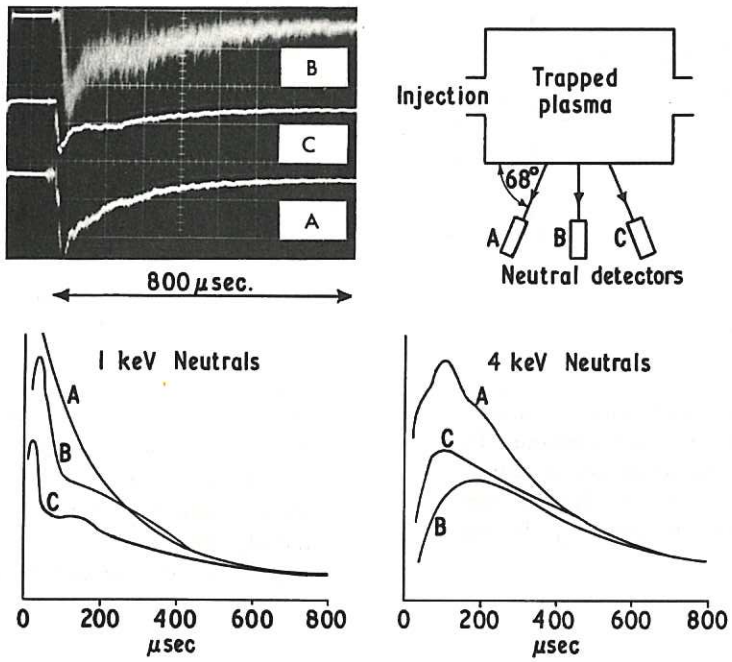

Fig.10 (CLM-P 245)

Neutral atom emission from the magnetic well. The position of the detectors A, B and C is as shown. The oscillograms are for 1 keV emission. The curves have been normalised to give the same amplitude at 600 μsec.

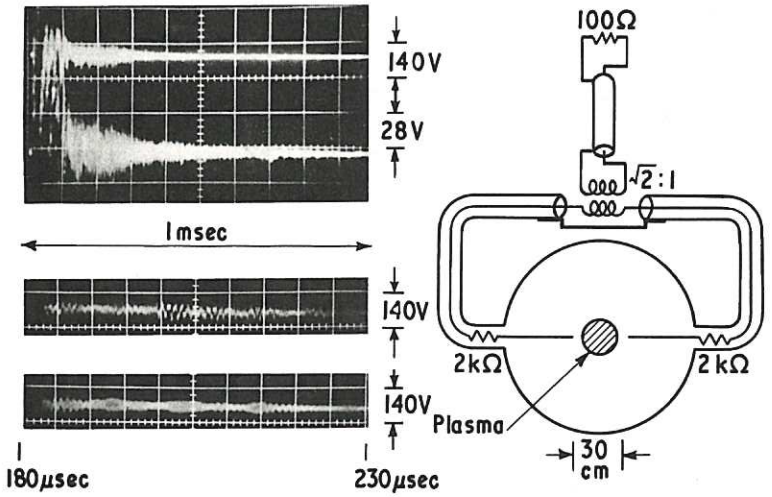

Fig.11 (CLM-P 245)

The measurement of high frequency potential fluctuations across the plasma diameter. The top oscillogram shows the same signal on two different sensitivities. The lower pair of oscillograms show the fluctuations on an expanded time scale.

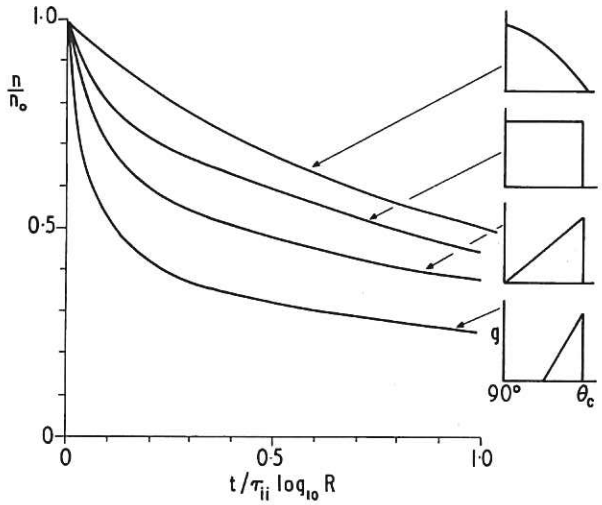

Fig.12 (CLM-P 245)
Density decay for the initial angular distribution shown. The curves were obtained by solving the diffusion equation for a mono-energetic distribution. τ_{ii} is the Spitzer ion-ion collision time initially and n_o is the initial density.

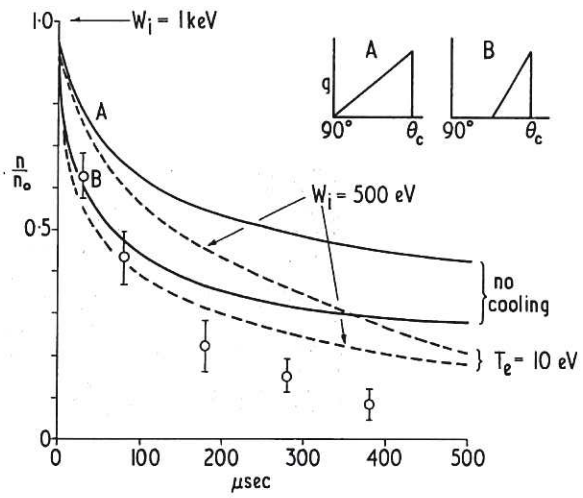

Fig.13 (CLM-P 245)
Density decay for the initial angular distributions A and B. Initial conditions are $W_i = 1$ keV and $n_o = 5 \times 10^{10}$ cm^{-3}. If $T_e = 10$ eV then $W_i = 0{\cdot}5$ keV at the times indicated. The error bars on the experimental points are of standard deviations of 10 shots.

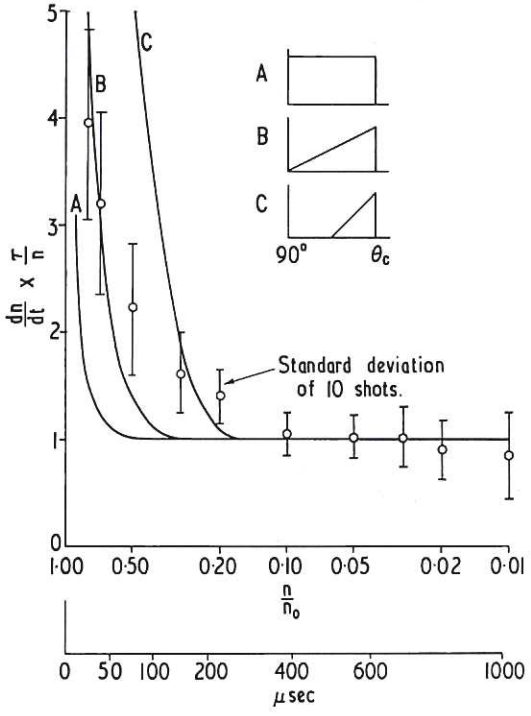

Fig.14 (CLM-P 245)
$(\tau/n)\,(dn/dt)$ against n/n_o for $\tau = 250\ \mu$sec. The solid curves show $F/\log_{10}R$ for the initial angular profiles A, B and C. The time scale shows the average time to reach any value of n/n_o.

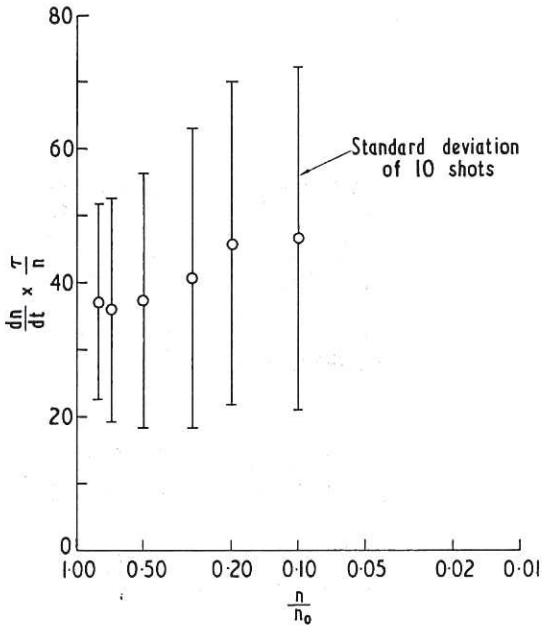

Fig.15 (CLM-P 245)
$(\tau/n)\,(dn/dt)$ against n/n_o for $\tau = \tau_{ii} \log_{10}R$. If the plasma decay were classical the experimental points would show the same behaviour as the solid curves in Fig.14.